IVYSPRING INTERNATIONAL PUBLISHER

Theranostics

2017; 7(5): 1072-1087. doi: 10.7150/thno.18193

Research Paper

Zero-order controlled release of BMP2-derived peptide P24 from the chitosan scaffold by chemical grafting modification technique for promotion of osteogenesis *in* vitro and enhancement of bone repair *in vivo*

Yan Chen[1*], Xujie Liu[2, 3*], Rui Liu[4*], Yong Gong[4], Mingbo Wang[5], Qianli Huang[6], Qingling Feng[6]✉, Bo Yu[4]✉

1. Department of Ultrasonic Diagnosis, Zhujiang Hospital of Southern Medical University, Guangzhou 510282, China;
2. Graduate School at Shenzhen, Tsinghua University, Shenzhen 518055, China;
3. State key laboratory of new ceramics and fine processing, Department of Materials Science and Engineering, Tsinghua University, Beijing 100084, China;
4. Department of Orthopedics, Zhujiang Hospital, Southern Medical University, Guangzhou 510282, China;
5. Key Laboratory of Biomedical Materials and Implants, Research Institute of Tsinghua University in Shenzhen, Shenzhen 518057, P. R. China;
6. Laboratory of Advanced Materials, Department of Materials Science and Engineering, Tsinghua University, Beijing 100084, China.

* These authors contributed equally to this work.

✉ Corresponding authors: Bo Yu: gzyubo@163.com; Qingling Feng: biomater@mail.tsinghua.edu.cn.

Received: 2016.11.03; Accepted: 2017.01.02; Published: 2017.02.27

Abstract

Combination of tissue-engineered bone scaffolds with cell-adhesive, osteoconductive, or osteoinductive biomolecules is a critical strategy to improve their properties that significantly influence cellular behaviors, such as adhesion, proliferation, and differentiation, which is beneficial for critical-sized bone defects repairing. However, the traditional surface modification techniques, such as physical adsorption, coating, and plasma treatment, et al, have great limitations for immobilization of bioactive molecules due to undesirable controlled delivery performance or overly complex multistep procedures. In this study, we functionalized the chitosan/hydroxyapatite (CS/HA) biomimetic composite scaffold for controlled delivery of BMP2-derived peptide (P24) by the chemical grafting modification technique: firstly, P24 was conjugated with a thiolated chitosan, chitosan-4-thiobutylamidine (CS-TBA); secondly, the resultant CS-P24 was then combined with HA to prepare CS-P24/HA scaffolds. The effect of CS-P24/HA scaffolds on bone regeneration was evaluated, along with the underlying biological mechanisms responsible *in vitro* and *in vivo*. *In vitro*, the controlled and sustained release of bioactive P24 could last up to 90 days, furthermore, the release profiles of CS-5%P24/HA and CS-10%P24/HA were linear and could be fitted according to zero-order kinetic model (R^2=0.9929; R^2=0.9757); P24 on the scaffold significantly promoted cell adhesion, proliferation, osteodifferentiation, and mineralization with synergistic effects. Bone marrow stromal cells (BMSCs) revealed spindle-shaped surface morphology, indicating the CS-P24/HA scaffolds supported cell adhesion and possessed a high proliferation rate that varied according to the P24 concentration levels. Furthermore, mRNA levels for OCN, Runx2, and collagen I were significantly up-regulated on CS-P24/HA scaffolds compared with cells grown on CS/HA scaffolds *in vitro* ($p < 0.05$). Similarly, the BMSCs exhibited a higher ALP expression and calcium deposition level on CS-P24/HA scaffolds compared with CS/HA scaffolds ($p < 0.05$). *In vivo*, osteoinductive studies revealed a significantly higher ectopic osteogenesis level of CS-10%P24/HA scaffolds in rat dorsal muscle pockets compared with that of CS/HA scaffolds. Finally, CS-P24/HA scaffolds showed superior performance in the reconstruction of rat calvarial bone defects. This novel CS-P24/HA scaffold is deemed a strong potential candidate for the repair of bone defects in human bone tissue engineering.

Key words: Controlled release, BMP2-derived peptide, thiolated chitosan, hydroxyapatite, scaffolds, bone defect repair.

Introduction

To improve the bone repairing efficacy of tissue-engineered bone scaffolds, it is feasible to modify the scaffolds with multiple bioactive agents, including cell adhesion-promoting peptides or proteins, osteoconductive particles, and osteoinductive growth factors or peptides. However, the traditional modification techniques, such as physical adsorption, usually can't achieve the long-term retention of growth factors owing to the weak interactions between biomolecules and biomaterials in the challenging biological environment. On the other hand, novel immobilization strategies, like coating and plasma treatment, electro-deposition, layer-by-layer, and electrostatic spinning, are not desirable due to their multistep procedures that are time consuming and may lead to inconsistent results with undesirable controlled delivery performance. Accordingly, an easy, simple, and effective technique is expectant and needed [1, 2]. Interestingly, thiolated chitosan comes into the field of vision. The modification of chitosan has been widely studied in order to get certain additional advantageous properties [3]. The amino groups of chitosan are target moieties for the modification of chitosan. The addition of thiol groups on the primary amino groups of chitosan, resulting thiolated chitosan, can improve some properties of chitosan [4]. Different from unmodified chitosan, which can only be dissolved in acid medium, the thiolated chitosan has good solubility at neutral pH. Moreover, the immobilized thiol groups are able to form disulfide bonds with other thiol groups in proteins, resulting in the improvement of mucoadhesion [5]. This novel system has the good stability and protein release properties due to the presence of thiol groups. Our previous study [6] demonstrated that thiolated chitosan/hydroxyapatite/β-glycerophosphate has a porous structure with a uniform distribution of nano-HA, an appropriate degradation rate, and low cytotoxicity, indicating potential applications in drug delivery systems and tissue engineering. However, thiolated chitosan based scaffold for BMP-2 peptide release has not been reported yet. It is important to study the BMP-2 peptide release behavior for the potential application of thiolated chitosan based scaffold in bone tissue engineering. Therefore, this has motivated us to attempt the fabrication of synergistic thiolated chitosan/HA to develop a controlled delivery system of BMP-2 peptides, which will be designed to not only provide effective delivery in a controlled and sustained manner but also simultaneously enhance the bioactivity of BMP-2 peptides.

BMP-2 was used to obtain osteoinductivity and enhance repair of critical-sized bone defects already [7], however, for the clinical therapy, it needs to be used in a high dosage, accompanied by a high cost, contingent risk and side effects such as excessive bone resorption [8] and promotion of tumor angiogenesis [9]. So far, delivering BMP-2 at a low but therapeutically efficient dose with minimal side effects was still one of the present challenges [10, 11]. In consideration of these noticeable issues of BMP-2 in biological function and controlled delivery, researchers attempted to seek for the most feasible solution from BMP-2-derived synthetic peptides. BMP-2-derived synthetic peptides were reported to possess the biological activity similar to that of natural BMP-2 and could induce ectopic bone formation [12, 13]. Some synthetic peptides, such as B2A2, consisting of a BMP receptor-targeting sequence, a hydrophobic spacer, and a heparin-binding sequence, can even synergically act with BMP-2 [14]. The P24 peptide was derived from the knuckle epitope of BMP-2. It consisted of small molecules and was chemically stable and structurally linear, facilitating exertion of its biological effects. P24 can regulate adhesion and differentiation of bone marrow stromal cells (BMSCs) and induce ectopic osteogenesis [15]. In addition, the P24 peptide, containing abundant aspartic acid and phosphorylated serine, can promote deposition of calcium and phosphate ions and accelerate nucleation and mineralization [16]. Moreover, P24 peptide is low-cost and suitable for cosmically production. With these popular characteristics, it seems to have the potential to expand the application space for BMP-2 peptide.

In this study, we developed a new biomimetic CS-P24/HA scaffold for the controlled and sustained delivery of BMP2-derived peptide P24 by chemical grafting modification technique. The objective of the present paper is to analyze the effect of the CS-P24/HA scaffold on bone regeneration and to examine the underlying mechanism *in vitro* and *in vivo*. First, we analyzed the physical and chemical properties of CS-P24/HA *in vitro*, including the P24 releasing curve. Then, we assessed the cell shape and proliferation of rat BMSCs on CS-P24/HA. Furthermore, ALP staining, ALP activity, calcium deposition, and osteogenic-specific genes (OCN and Runx2) of BMSCs cultured on the scaffolds were analyzed. Finally, we surgically created heterotopic ossification and a calvarial bone defect model in rats and investigated the efficacy of the CS-P24/HA scaffold for inducing new bone formation and regeneration.

Materials and methods

Materials

Chitosan (CS, viscosity: 50–800 mPa•s, degree of de-acetylation: 80%–95%) was purchased from Sinopham Chemical Reagent Co., Ltd, China. Peptide 24 (P24) derived from BMP-2 (N→C: KIPKA SSVPT ELSAI STLYL SGGC) was synthesized by Shanghai ZiYu Biotech Co., China. 2-iminothiolane hydrochloride and dimethyl sulfoxide (DMSO) were purchased from Sigma-Aldrich, USA.

Immobilization of peptide on chitosan through thiol groups

Thiolated chitosan was prepared with 2-iminothiolane by previously described method [6]. Briefly, 40 mg of 2-iminothiolane hydrochloride was added to 200 mL of 0.2% (w/v) chitosan solution (in 1% acetic acid). The pH was adjusted to 6 with 5 M NaOH. After continuous stirring at room temperature for 24 h, the resulting thiolated chitosan polymer conjugate was dialyzed against 5 mM HCl once, 5 mM HCl containing 1% NaCl twice, 5 mM HCl once, and finally 1 mM HCl once, and then lyophilized at −50 °C and 20 Pa. The synthesized peptide was terminated with cysteine. The thiol group in cysteine can form a di-sulfide bond with the thiol group in thiolated chitosan by DMSO according to a previous procedure [17]. The resultant thiolated chitosan was dissolved in 60 mL of de-ionized water at a concentration of 0.5% (w/v). The synthesized peptide (5% or 10% of the weight of chitosan in 15 mL DMSO) was added into the thiolated chitosan solution. After continuous stirring at room temperature for 4 h, the mixture was dialyzed against de-ionized water for 5 days and lyophilized at −50 °C and 20 Pa in order to immobilize the peptide within the chitosan (Chitosan-Peptide 24, CS-P24).

Characterization of CS-P24

FT-IR (Nicolet 6700FTIR, Thermo Fisher Scientific,USA) was employed to characterize the structure of CS-P24, CS, and P24. The IR spectra of CS-P24, CS, and P24 were recorded at room temperature using the KBr pellet technique. An IR spectral range of 400–4000 cm^{-1} was analyzed for each sample.

Preparation of CS-P24/HA scaffold

200 mg of CS-P24 was hydrated in 10 mL 0.1M HCl. HA powder (200 mg) (obtained from Institute of Nuclear and New Energy Technology, Tsinghua University) was added with continuous stirring until uniformly distributed. Thereafter, the hybrid of CS-P24 and HA was lyophilized at −50 °C and 20 Pa using a 96-well plate (Corning, USA) as a mold to obtain the CS-P24/HA scaffold. CS was used instead of CS-P24 as a control (CS/HA scaffold) and different amounts of P24 (5% or 10% of the weight of CS: CS-5%P24/HA or CS-10%P24/HA scaffold) were used with both *in vitro* and *in vivo* tests.

Characterization of CS-P24/HA scaffold

To characterize the scaffold with electron microscopy, the CS-P24/HA scaffold was sputter-coated with gold and observed by a scanning electron microscope (SEM, JSM-7001F, Japan). The porosity of the CS-P24/HA scaffold was measured by a mercury intrusion analyzer (Autopore IV 9510, Micromeritics, USA). The element composition and chemical states analysis of CS/HA, CS-5%P24/HA, and CS-10%P24/HA scaffolds were determined by X-ray photoelectron spectroscopy (XPS, ESCALAB-250Xi) equipped with a monochromatic Al Kα X-ray source. The binding energy was calibrated with C1s = 284.8 eV. Both N 1s and S 2p high-resolution spectra were recorded with a pass energy of 20 eV and an energy resolution of 0.05 eV. The P24 release profiles of CS-P24/HA scaffold were determined in vitro by high performance liquid chromatography system (HPLC, Shimadzu 10Avp, Japan). The CS-P24/HA samples were immersed in 5.0 mL sterile PBS solution and incubated at 37 °C under continuously shaking (40 rpm) for 90 days. At designated time points, the supernatant was collected and resuspended in the fresh PBS. The amount of P24 in the obtained supernatant was then measured by HPLC. All experiments were performed in triplicate for each of the samples.

Rat BMSC isolation

Rat BMSCs were isolated from the femurs and tibias of eight-week-old female SD rats as described elsewhere [18]. Cells were cultured in DMEM supplemented with 15% fetal bovine serum (Gibco) and 1% penicillin-streptomycin liquid (100 U/mL) (Gibco). Cell passage numbers P4 and P6 were utilized for all experiments.

Observation of cell morphology

BMSCs were seeded onto CS/HA, CS-5%P24/HA, and CS-10%P24/HA at 2 × 10^4 cells/cm^2 and cultured in DMEM supplemented with 15% fetal bovine serum, 1% penicillin-streptomycin liquid (100 U/mL). The medium was exchanged every 3 days. After five days of culture, specimens were fixed by 0.25% glutaraldehyde solution for 24 h. After rinsing 3 times in 1× PBS, the specimens were immersed in OsO4 (Ted Pella) for 1 h and then subsequently rinsed 3 times in 1x PBS. The specimens were then dehydrated with increasing concentrations

of acetone (30–100% v/v). After drying, the specimens were mounted on aluminum stubs and then viewed under SEM (Hitachi S-3000N, Japan) at an accelerating voltage of 20 kV.

Cell proliferation assay

The proliferation of BMSCs was measured by the Cell Counting Kit-8 (CCK-8, Dojindo). Cells were cultured on the CS/HA, CS-5%P24/HA, and CS-10%P24/HA scaffolds for 1, 3, 7, and 10 days in DMEM supplemented with 15% fetal bovine serum and 1% penicillin-streptomycin liquid (100 U/mL) and then incubated in 10% CCK-8 solution in a 5% CO_2 incubator at 37 °C for 4 h. The absorbance of the culture medium was then measured at 450 nm.

Fluorescence microscopy

Rat BMSCs were seeded onto the CS/HA, CS-5%P24/HA, and CS-10%P24/HA scaffolds at 2 × 10^4 cells/cm^2. After culturing for 1, 3, and 7 days in DMEM supplemented with 15% fetal bovine serum, 1% penicillin-streptomycin liquid (100 U/mL), specimens were fixed in 4% formalin solution for 15 min and 0.3%Triton X-100 in 1x PBS for 10 min, cell nuclei were visualized by DAPI (Beyotime Institute of Biotechnology) and viewed under a confocal microscope system (Olympus, BX61W1-FV1000, Japan).

Alkaline phosphatase (ALP) activity determination

As an index for *in vitro* osteogenic differentiation of BMSCs during growth on the novel thiolated chitosan scaffolds, ALP activity was determined. After co-culture for 3, 7, and 10 days, the seeded scaffolds were treated with 1.0 mL of Triton X-100 cell lysis medium overnight at 4°C, followed by removal of all liquid. The ALP activity in each well was assayed using an ALP optimized test kit (Nanjing Jiancheng, China), according to the manufacturer's procedures. The absorbance was measured at an excitation/emission of 520 nm on a plate reader.

Calcium deposition of BMSCs

BMSCs (2 × 10^4/cm^2) were seeded onto the scaffolds and cultured in DMEM supplemented with 15% fetal bovine serum and 1% penicillin-streptomycin liquid (100 U/mL). After 14 days, to identify calcium deposition, Alizarin Red S staining was conducted. The medium was removed and the cells washed with ddH_2O and fixed in 4% paraformaldehyde for 10 min at room temperature. After gently rinsing with ddH_2O, the cells were stained in a solution of 2% Alizarin Red S at pH 4.1 for 20 min and then washed with ddH_2O. The samples were air dried and the calcium deposition area was analyzed with photomicrographs in Image-J for five randomly selected fields under an optical microscope (Olympus IX71, Japan).

Alkaline phosphatase (ALP) staining

BMSCs (2 × 10^4/cm^2) were seeded onto the scaffolds and cultured in DMEM supplemented with 15% fetal bovine serum and 1% penicillin-streptomycin liquid (100 U/mL). After 14 days, ALP staining was performed using a cell alkaline phosphatase stain cAKP kit (Nanjing Jiancheng Bioengineering Institute). The ALP-positive area was observed under an optical microscope (Olympus IX71, Japan).

Real-time polymerase chain reaction (PCR) conditions

The levels of mRNA for osteogenic specific genes (OCN and Runx2) and the related matrix gene collagen 1 (Col 1) of rat BMSCs cultured on the scaffolds in DMEM supplemented with 15% fetal bovine serum and 1% penicillin-streptomycin liquid for 1, 3, and 7 days were assessed using real-time PCR. Total cellular RNA was isolated by lysis in TRIzol (Invitrogen Inc., Carlsbad, CA, USA). PCR was performed using the Transcriptor cDNA Synth Kit and FastStart Universal SYBR Green Master (Roche). PCR consisted of 40 cycles of amplification of the template DNA with primer annealing at 60 °C. The relative level of expression of each target gene was then calculated using the $2^{-\Delta\Delta Ct}$ method. The amplification efficiencies of primer pairs were validated to enable quantitative comparison of gene expression. All primer sequences (Invitrogen Inc., Carlsbad, CA, USA) were designed using primer 5.0 software. Each real-time PCR was performed on at least three different experimental samples and representative results are showed as target gene expression normalized to the reference gene β-actin. Error bars reflect one standard deviation from the mean of technical replicates.

In vivo ectopic bone formation experiment

Implantation experiment in SD rats

All animals in this study were managed under an approved IRB protocol. In this study, 18 healthy female Sprague–Dawley (SD) rats (average weight 150 g), supplied by the Animal Research Center of Guangdong Province, were divided into three equal groups (A, B, and C). After induction with midazolam, the rats were anesthetized with a 0.3 mL/kg mixture of xylazinesecobarbital and ketamine (2:1). Rats were then placed in the prone position, depilated, and sterilized from the arcus costarum to

the hip joint. An incision was made close to erector spinae. We performed blunt dissection on superficial fascia and created two muscle pouches in either side of the back. Rats in groups A, B, and C were, respectively, implanted with CS/HA, CS-5%P24/HA, and CS-10%P24/HA. For each rat, two scaffolds of the same type were implanted. The administration of antibiotics as a prophylactic measure was carried out. All animals survived to the designated time point without any major complications. The rats were sacrificed at weeks 4, 8, and 12 post-surgery, and the implants together with surrounding tissues were harvested and fixed immediately with 10% neutral formalin.

Micro-CT measurement

The harvested specimens for weeks 4, 8, and 12 were immediately fixed in 10% (v/v) neutral buffered formalin for 24 h. For determination of the 3D architecture of the subcutaneous scaffold harvested from the back of each rat, animals were sacrificed, and specimens were harvested and analyzed in an advanced micro-computed tomography instrument (ZKKS-MC-Sharp-IV, Zhongke Kaisheng Bio, Inc.). A three-dimensional reconstruction of the images was done with the region of interest containing the scaffold. Histomorphometric parameters, including bone mineral content (BMC), bone mineral density (BMD), and tissue mineral density (TMD), were evaluated.

Histological examination

The harvested specimens for weeks 4, 8, and 12 were immediately fixed in 10% (v/v) neutral buffered formalin for 24 h, and de-calcified in neutral 10% EDTA solution for one week at room temperature. Samples were de-hydrated with an alcohol gradient, cleared, and embedded in paraffin blocks. Histological sections (5 μm) were prepared using a microtome and subsequently stained with hematoxylin and eosin (HE). The stained sections were photographed digitally under a microscope.

Immunohistochemistry

To analyze *Ocn, CD31* and *Nestin* expression of the tissue, immunohistochemical staining was performed on paraffin sections. The primary antibodies were rabbit anti-rat *Ocn, CD31* and *Nestin* monoclonal antibody (Abcam). The specimens were then incubated with goat anti-rabbit second antibodies conjugated with HRP (Boster Company of Biotechnology). The antibody complexes were visualized by the addition of a buffered diaminobenzidine (DAB) substrate for 20 s and Mayer's haematoxylin was used for counter staining. The stained specimens were photographed digitally under a microscope.

In vivo calvarial defect repair experiment

Animal model

Sixteen female two-month-old SD rats (250-300 g, average 280 g) (Center of Experimental Animals of Guangdong Province) were utilized for this experiment with approval from The Southern Medical University Institutional Animal Care and Use Committee approved the study protocol. Under general anesthesia, the cranium was exposed through a medial incision. Bilateral full-thickness circular defects (5 mm in diameter, 1 mm in thickness) were generated by a dental bur. Size of bilateral calvarial defects in the present study was under the protocol of the previously reported studies [19-21]. The defects were implanted with CS/HA, CS-5%P24/HA, and CS-10%P24/HA. The control groups were left untreated. In all animals, the wound was then irrigated and fascia and skin were closed. Post-operatively, animals were allowed free cage activity. The whole calvarias were harvested for evaluation after both 4 and 8 weeks of implantation.

Micro-CT measurement of calvarial defect repair

The harvested specimens for both 4 and 8 weeks were immediately fixed in 10% (v/v) neutral buffered formalin for 24 h. For determination of 3D architecture of the calvarial bone sample harvested from the back of each rat, animals were sacrificed, and specimens were harvested and analyzed in an advanced micro-computed tomography instrument (ZKKS-MC-Sharp-IV, Zhongke Kaisheng Bio, Inc.). A three-dimensional reconstruction of the images was performed with a 4 mm region of interest containing the scaffold. Histomorphometric parameters, including bone mineral density (BMD) and trabecular number (Tb.N) were evaluated.

Histological examination

The harvested specimens for both 4 and 8 weeks were immediately fixed in 10% (v/v) neutral buffered formalin for 24 h, and de-calcified in neutral 10% EDTA solution for one week at room temperature. Samples were dehydrated through an alcohol gradient, cleared, and embedded in paraffin blocks. Histological sections (5 μm) were prepared using a microtome and subsequently stained with hematoxylin and eosin (HE) or Masson's trichrome staining. The stained sections were photographed digitally under a microscope.

Immunohistochemistry of SD rat tissue

To analyze *osteocalcin* (*Ocn*) and *CD31* expression

of the tissue, immunohistochemical staining was performed on paraffin sections. The primary antibodies were a rabbit anti-rat *Ocn* and a monoclonal *CD31* antibody (Abcam). The specimens were then incubated with goat anti-rabbit secondary antibodies conjugated with HRP (Boster Company of Biotechnology). The antibody complexes were visualized by the addition of a DAB substrate for 20 s and Mayer's haematoxylin was used for counterstaining. The stained specimens were photographed digitally under a microscope.

Statistical analysis

All quantitative data are presented as mean ± SD. The student's t-test was performed to assess statistical significance of results between groups. Values of $p < 0.05$ were accepted as statistically significant. Significance level was presented as either $*p < 0.05$ or $**p < 0.01$.

Results

Preparation of CS-P24

2-iminothiolane has been widely used to react with primary amines in CS [22, 23]. The resulting thiolated CS showed a good solubility in water, which made it proper for the subsequent coupling reaction with peptide terminated with cysteine (containing thiol groups), as shown in Fig. 1A. FT-IR spectra of CS, P24, and CS-P24 are shown in Fig. 1B. The main peaks of un-modified CS were as follows: the strong and broadband centered at 3381 cm^{-1} (N–H stretch and O–H stretch), the peak at 2875 cm^{-1} (C–H stretch), 1655 cm^{-1} (C=O stretch), 1597 cm^{-1} (N–H blend), 1155 cm^{-1} (bridge O stretch), 1080 cm^{-1} (C–H stretch), and 895 cm^{-1} (the β(1→4) glycoside bridge structure) [23-26]. For the spectrum of CS-P24, the typical amide I bond at 1633 cm^{-1} and the amide II band at 1531 cm^{-1} were detected, which also existed in the spectrum of P24, indicating that P24 had been immobilized on CS [27, 28].

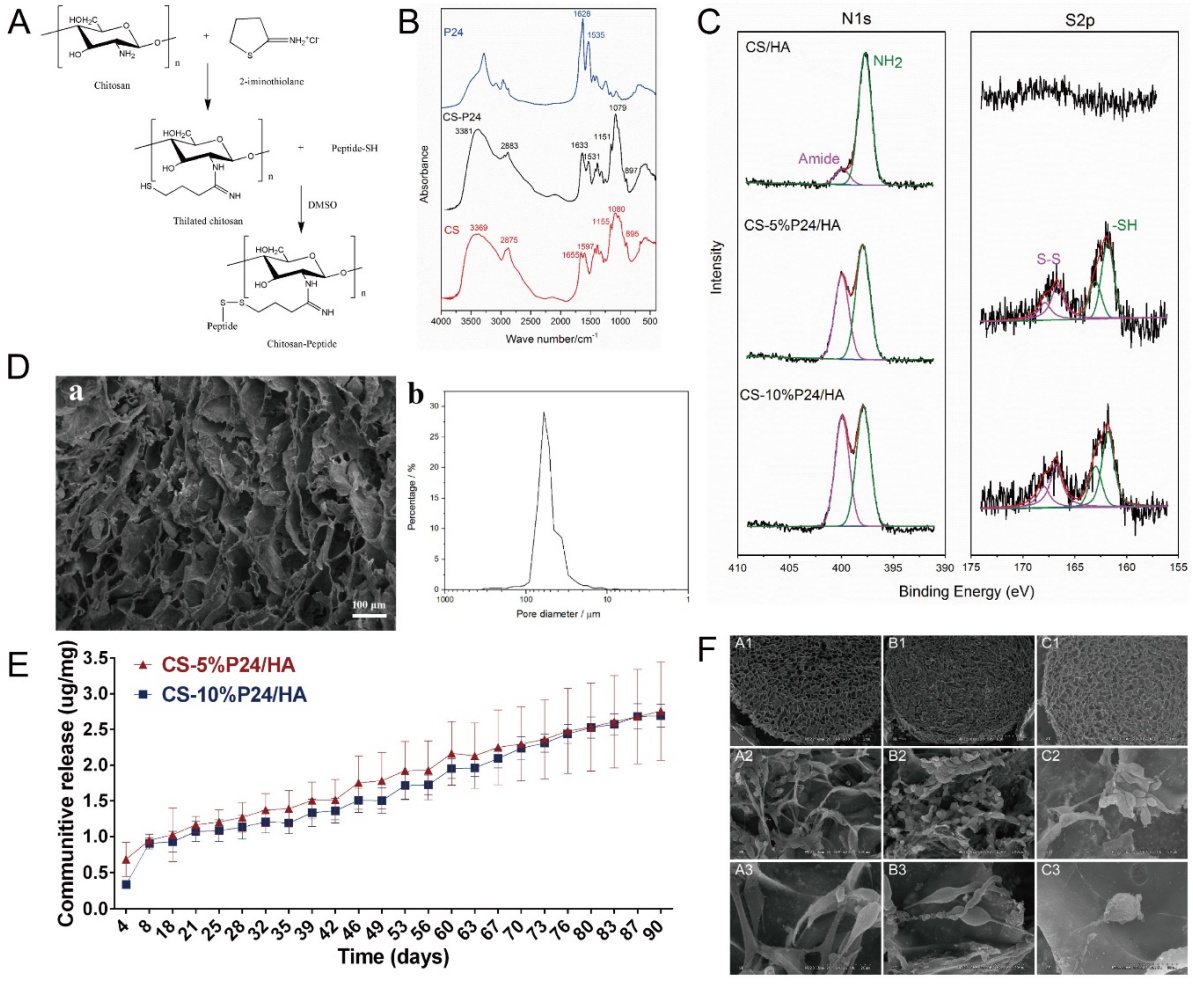

Figure 1. (A) Synthesized thiolated chitosan and chitosan peptide. (B) FTIR spectra of CS, P24, and CS-P24. (C) N1s and S2p high-resolution XPS spectra of CS/HA, CS-5%P24/HA, and CS-10%P24/HA scaffolds. (D) SEM image (a) and distribution of pore diameter (b) of CS-P24/HA scaffold. (E) Cumulative *in vitro* release curves of the CS-P24/HA scaffolds over a period of 90 days. Data were obtained using an ELISA assay. Error bars represent means ± SD ($n = 3$). (F) Scanning electron microscope (SEM) images of (A1-A3) CS/HA, (B1-B3) CS-5%P24/HA, and (C1-C3) CS-10%P24/HA. (A1, B1, C1) SEM images of the porous biomaterial (30×). (A2, B2, C2) Scaffolds adhered with BMSCs (500×). (A3, B3, C3) The surface of the scaffolds with complex 3D structures (2000×).

Characterization of CS-P24/HA scaffold

The CS-P24/HA scaffold showed a highly porous inner structure, which could be observed by SEM (Fig. 1D). The porosity of the scaffold as determined by mercury intrusion analyzer was 95.7%. The network formed by chitosan was not smooth but attached by the nano-HA particles, confirmed by the existence of calcium in the energy diffraction spectrum (EDS, data not shown). Fig. 1D showed the distribution of the pore diameters of the CS-P24/HA scaffold determined by mercury intrusion analyzer. The majority of the pores had a diameter from 30–90 μm and the median pore diameter by volume was 59.8 μm. XPS was employed to characterize the chemical compositions and states of scaffolds with varying amounts of P24 (Fig. 1C). The differences in the N1s and S2p spectra were observed for different scaffolds. As expected, no obvious peaks were detected in the CS/HA scaffold, indicating the absence of a sulfur element. For CS-5%P24/HA and CS-10%P24/HA, the S2p spectra both had a doublet structure due to the presence of the S2p3/2 and S2p1/2peaks, which could be fitted using a 2:1 peak area ratio and a 1.2 eV splitting. The two peaks of S2p3/2 (S2p1/2) implied two different chemical states of sulfur: the peak at 161.8 eV (163.0 eV) for free thiol groups and the peak at 166.8 eV (168.0 eV) for di-sulfide bonds. The S/C ratio for CS-5%P24/HA and CS-10%P24/HA was 0.64% and 0.92%, respectively. For N1s, the spectra for all of the three scaffolds could be divided into two components: a component at 397.7 eV corresponding to amino acids [29, 30] and a component at 399.9 eV corresponding to amides [31]. The amide in chitosan was due to the in-complete de-acetylation. The high amount of amide in CS-P24 was mainly assigned to the existence of the peptide. The increase of the peak intensity for the amide and S/C ratio from CS-5%P24/HA to CS-10%P24/HA both demonstrated the increasing amount of P24 in the scaffolds.

Release behaviors of the BMP2-derived peptide P24

BMP2-derived peptide P24 with different doses was loaded into the scaffolds. The *in vitro* cumulative release curves of P24 from the scaffolds over a period of 90 days were shown in Fig. 1E. In the absence of a burst release profile, the release of BMP2-derived peptide P24 was stable for the entire length of time assayed (90 days). Furthermore, the release profiles of CS-5%P24/HA and CS-10%P24/HA were linear and could be fitted according to zero-order kinetic model (R^2=0.9929; R^2=0.9757). The release rates of BMP-2-derived peptide P24 of CS-5%P24/HA and CS-10%P24/HA were almost equal over 90 days. The peptide P24 cumulative release of CS-10%P24/HA scaffold was lower than that of the CS-5%P24/HA scaffold at each time point. Compared to the CS-5%P24/HA scaffold, the CS-10%P24/HA scaffold had a higher peptide P24 concentration and lower peptide P24 cumulative release, which facilitated the larger sustained diffusion of protein molecules into the release medium over a relatively long period of time. Our results suggested the CS-P24/HA scaffolds could efficiently release peptide P24 in a control and sustained profile.

Morphology and proliferation of BMSCs on scaffolds

To determine the effect of the scaffolds on cell growth, BMSCs were seeded onto CS/HA, CS-5%P24/HA, and CS-10%P24/HA scaffolds. Cell morphology was observed by SEM 5 days after seeding (Fig. 1F). The SEM micrographs indicated that most of the BMSCs exhibited a spindle morphology on CS/HA, CS-5%P24/HA, and CS-10%P24/HA (Fig. 1F: A3, B3, and C3). After 5 days of culture, there was a large amount of BMSCs observed on CS/HA, CS-5%P24/HA, and CS-10%P24/HA scaffolds (Fig. 1F: A2, B2, and C2). Cell proliferation was measured by the CCK-8 assay (Fig. 2A). CCK-8 analysis showed that the cell number significantly increased in both CS-10%P24/HA and control group scaffolds (Fig. 2A). The CS-10%P24/HA group had significantly higher optical values than CS/HA group at days 1, 3, and 7 ($p < 0.05$) (Fig. 2A). In addition, adhesion of BMSCs to CS/HA and CS-P24/HA scaffolds was further studied by DAPI nuclear staining (Fig. 2B). The numbers of DAPI stained cells in four groups increased over time. As shown, the density of BMSCs on the CS-P24/HA scaffold was higher than that of the CS/HA scaffold on days 3 and 7 (Fig. 2B), which was consistent with the results indicated by the CCK-8 test. The good cytocompatibility of the CS-P24/HA scaffold was attributed to its improved hydrophilicity, flexibility, and surface patterned microstructure. Appropriate hydrophilic surfaces would be more conducive to initial cell attachment. From these comparisons, we demonstrated that the CS-P24/HA scaffolds were non-cytotoxic to BMSCs. Collectively, our results suggested that the CS-P24/HA scaffolds supported a better morphology and proliferation pattern of BMSCs compared to the CS/HA scaffold.

Effects of the CS-P24/HA scaffolds on the osteogenic differentiation of BMSCs

Osteogenic differentiation by BMSCs within the CS-P24/HA scaffolds was examined by ALP activity, ALP staining, and Alizarin Red S staining. The results showed that, for each group, the highest ALP activity

of BMSCs appeared on day 7. On day 10, the ALP activity of BMSCs decreased among the control, CS/HA, and CS-5%P24/HA group, but still maintained a relatively high level in CS-10%P24/HA group ($p < 0.05$) (Fig. 2C). Alizarin Red S staining showed evidence of calcium deposition and nodule formation. Although mineralized nodules were observed in all groups, more distinct nodules were observed in BMSCs stimulated by the CS-P24/HA scaffolds on day 14 (Fig. 2D). ALP staining showed that the cells in each group accumulated to form multiple layers and were polygonal and cubic shaped after 14 days of culture. Deposition of red brown particles was found in the cytoplasm of ALP-positive cells. However, ALP positive cells or calcified nodules were found more frequently on the CS-P24/HA scaffold groups on day 14 compared to the other groups (Fig. 2E).

Real-time polymerase chain reaction

To further examine the effect of the CS-P24/HA scaffold on osteogenic differentiation of BMSCs, we examined osteogenic gene expression (Fig. 2F). Osteogenic specific genes (OCN and Runx2) and related matrix genes collagen 1 (Col-I) were assessed. Both expressions of OCN and Runx2 were higher for CS-P24/HA than that for the control groups on days 1, 3, and 7. OCN remarkably increased 10.2-fold and 1.7-fold on CS-5%P24/HA compared with those of control ($p < 0.05$) and CS-10%P24/HA groups ($p < 0.05$) on day 3, respectively. The same trend was observed in the osteogenic transcription factor Runx2, with a 3.8-fold and 2.4-fold higher expression than those of control ($p < 0.05$) and CS-10%P24/HA groups ($p < 0.05$), respectively. The OCN and Runx2 expression levels of the CS-P24/HA groups were markedly up-regulated on days 3 and 7 ($p < 0.05$) and reached relatively high levels. Col-I expressions in CS-5%P24/HA and CS-10%P24/HA were lower than the control group on day 1 and 3 ($p < 0.05$). However, the mRNA transcript levels of Col-I in CS-10%P24/HA (15.6-fold, $p < 0.05$) was increased significantly compared to that of control group on day 7. Taken together, these results demonstrated that the CS-P24/HA scaffolds could promote the osteogenesis *in vitro*.

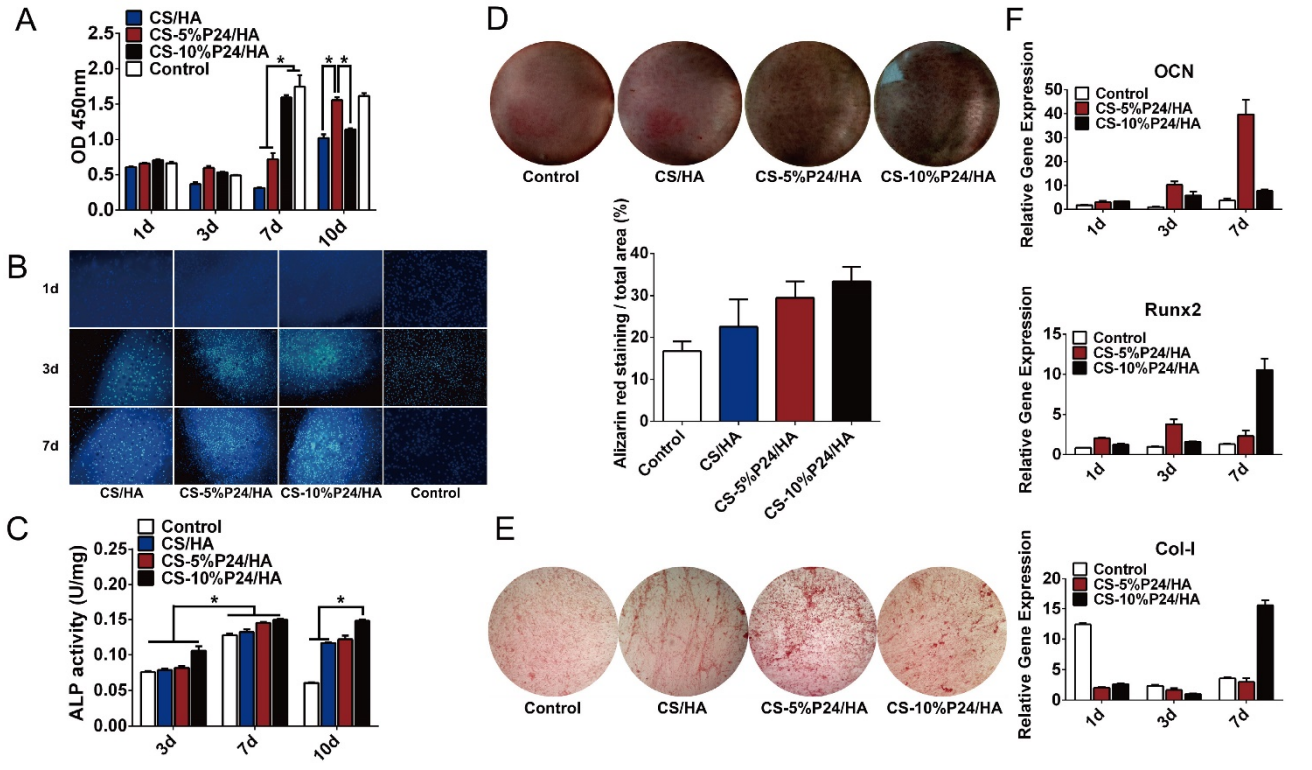

Figure 2. (A) CCK-8 test of BMSC viability after co-culture with CS/HA, CS-5%P24/HA, and CS-10%P24/HA scaffolds at days 1, 3, 7, and 10 ($p < 0.05$). (B) Images show the adhesion of BMSCs seeded on CS/HA, CS-5%P24/HA, and CS-10%P24/HA scaffolds at days 1, 3, and 7. Nuclei were stained with DAPI and images were captured at a 100× magnification. (C) The relative ALP activity of BMSCs cultured in a scaffold-stimulated medium. (D) Alizarin Red S staining of BMSCs cultured scaffold-stimulated medium. (E) The ALP staining of BMSCs cultured in scaffold-stimulated medium. (F) The level of the mRNA for osteogenic-specific genes (OCN and Runx2) and related matrix genes collagen 1 (Col 1) of rat BMSCs cultured on CS-P24/HA scaffolds for 1, 3, and 7 days. Levels, quantified using real-time RT-PCR, are normalized to the reference gene β-actin. (*$p < 0.05$); Error bars represent means ± SD (n = 3).

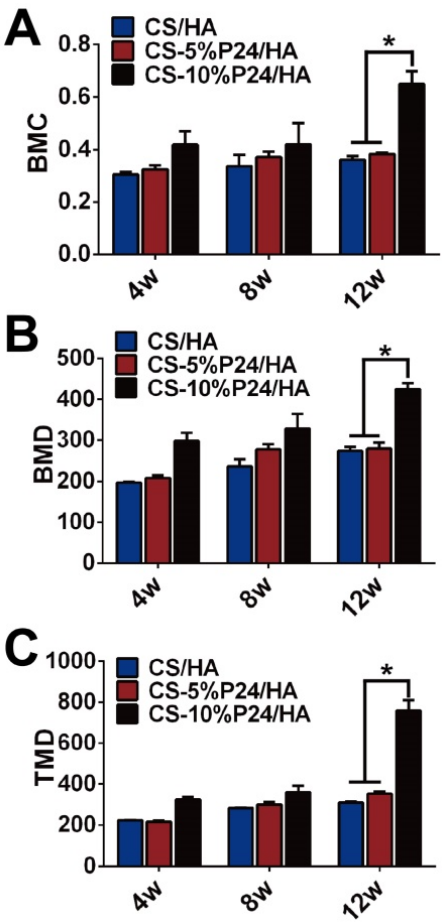

Figure 3. Quantitative analysis of mineralized new bone formation from micro-CT at 4, 8, and 12 weeks. (A) Bone mineral content (BMC). (B) Bone mineral density (BMD). (C) Tissue mineral density (TMD). *$p < 0.05$.

Ectopic bone formation of scaffolds in rats

Micro-CT evaluation of implanted scaffolds

The ectopic bone formation of the CS-P24/HA scaffolds in the back muscle pouches of living rats was quantitatively evaluated by determining the bone parameters of the implants. The three groups all displayed new bone formation as indicated by BMC, BMD, and TMD. The values of the bone parameters (BMC, BMD, and TMD) of the implants increased over time in all three groups. The CS-10%P24/HA group showed higher BMC, BMD, and TMD levels compared to those of the CS-5%P24/HA group and the CS/HA group (Fig. 3). The CS-10%P24/HA scaffold produced obvious bone formation in the back muscle pouches of rats and so fostered more extensive mineralization in the implants. This led to high BMD values, suggesting that the sustained release of BMP-2 peptide from the CS-10%P24/HA scaffold was of great benefit to osteoblast differentiation during early stages and subsequently promoted ectopic bone formation. However, the CS-5%P24/HA group and the CS/HA group showed no significant difference with respect to BMD, BMC, and TMD values at 8 and 12 weeks, attesting that BMP-2-containing scaffolds might not lead to difference in ectopic bone formation of rats unless the BMP-2 dose was at a particular threshold.

Histology

Tissue infiltration had fully occurred 4 weeks post-implantation in all scaffolds as shown in Fig. 4A. The connective tissue had infiltrated the scaffolds and the macrophages could be observed. The tissue morphology remained constant over the full course of the implantation period and no obvious decrease in the macrophage number was observed from 4 to 12 weeks post-implantation. In the CS-P24/HA groups, the mineralized tissue gradually filled the scaffolds and bone formation started at the periphery of the scaffolds, whereas it also initiated in the core of the scaffold for the CS-P24/HA specimens. Obviously, the center of the CS-P24/HA scaffolds region was composed mostly of collagen and calcium chloride (Fig. 4A). Immunohistochemistry targeting osteocalcin (OCN), CD31, and Nesting were performed. Osteocalcin was expressed in the bone matrix and was more intense at 8 and 12 weeks post-implantation. Osteocalcin was mainly expressed in the osteoblast lacunae, at the ossification line or even in the surrounding soft tissue (Fig. 4B). Newly formed blood vessels could be seen 4 weeks after implantation. A multitude of blood vessels were also observed throughout the entire thickness of the scaffolds. The CS-P24/HA group had higher numbers of OCN-positive osteoblasts and larger CD31-positive areas than the CS /HA group at weeks 4, 8, and 12 (Fig. 4C). Vessel formation might enhance the bone formation in the inner area of the scaffold. Nesting-positive BMSCs were obviously seen surrounding the scaffolds in CS-P24/HA group but rarely seen in the CS/HA group (Fig. 5), suggesting that BMSCs played a special role in the CS-P24/HA-induced ectopic bone formation.

In vivo calvarial defect repair experiment

X-ray

Bone-like tissue was formed in the defect areas at both 4 and 8 weeks after implantation, as revealed by X-ray scanning images (Fig. 6A). High-density shadows in the middle of the defect and at the edge of the calvarial defects were observed in the CS-5%P24/HA group and the CS-10%P24/HA group at 4 weeks, indicating a limited amount of new bone mineralized nodules and bone islands, whereas the blank control group did not exhibit evidence of any new bone formation. The whole defect was mostly

repaired by bone-like tissue at 8 weeks in the CS-P24/HA groups. Interestingly, the new bone was formed not only on the edge of the defect but also in the center. However, only small bone-like or vague radiopaque tissue was detected in defects of the CS/HA group at 8 weeks. Radiopaque tissue was almost undetectable in the blank group at 4 weeks and only minimal bone-like tissue was detected at 8 weeks. The opacity volume in the defect was elevated in the CS-P24/HA groups than that in the CS/HA group at 4 and 8 weeks.

Micro-CT

The calvarial bone repair was further evaluated by the micro-CT analysis at 4 and 8 weeks (n = 4) (Fig. 6B, 6C). In the CS-P24/HA group, the bone islands and in-growth of new bones emerged at 4 weeks, with the formation of new bone that filled the majority of the defect area at 8 weeks. The sagittal view demonstrated signs of bone bridging, while the coronal view suggested similar bone density inside and outside the defects at 8 weeks. The 3D rendering images confirmed substantial bone healing in the

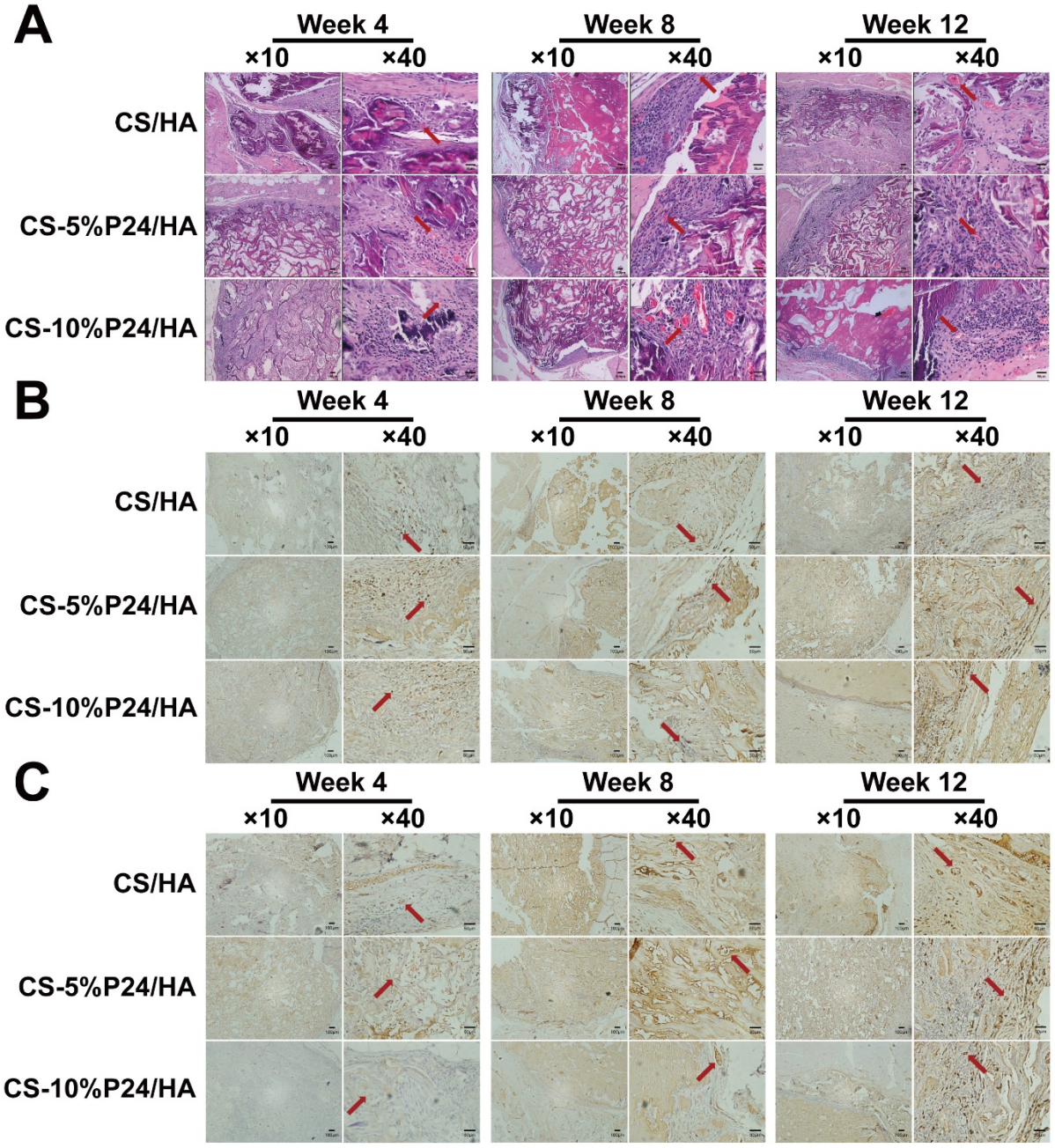

Figure 4. (A) Histology of the specimens after 4, 8, and 12 weeks after implantation *in vivo*. Hematoxylin and eosin staining of harvested tissues in CS/HA, CS-5%P24/HA, and CS-10%P24/HA groups. Red arrows show new formed blood vessels in or around the scaffolds. (B) Immunohistology. Cells or area in dark brown represent OCN-positive cells, and the areas in white are voids. (C) Immunohistology. Area in dark brown is positive area of CD31, indicating the blood vessels, and the areas in white are voids. The representative images at 10× magnification and at 40× magnification are presented. (At 10× magnification, scale bar = 100 μm. At 40× magnification, scale bar = 50 μm.)

CS-10%P24/HA group at 8 weeks. In contrast, the bone repair was slow and poor in the CS/HA group (Fig. 6B). Based on the micro-CT analysis, BMD and Tb.N were highest in the CS-10%P24/HA group at 4 and 8 weeks (Fig. 6C). In contrast, the BMD and Tb.N in the blank and the CS/HA group remained at a lower level at 4 and 8 weeks. The representative images and quantitative analyses likewise showed that the CS-10%P24/HA scaffold triggered better bone repair than the CS/HA group at 4 and 8 weeks, attesting that P24 was effective for calvarial bone healing.

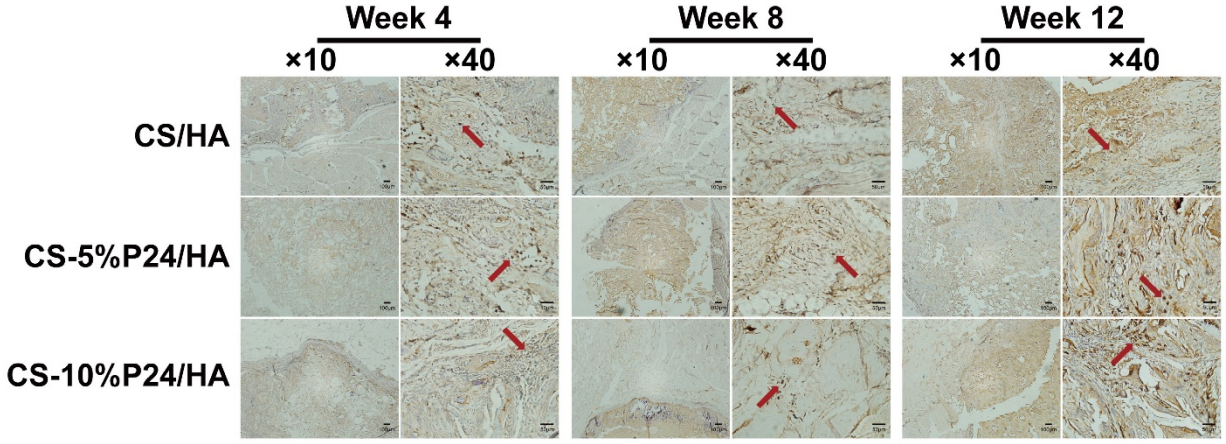

Figure 5. Immunohistology. Nesting expressed of the harvested tissues at 4, 8, and 12 weeks after implantation *in vivo*. The representative images at 10× magnification and at 40× magnification are presented. (At 10× magnification, scale bar = 100 μm. At 40× magnification, scale bar = 50 μm.)

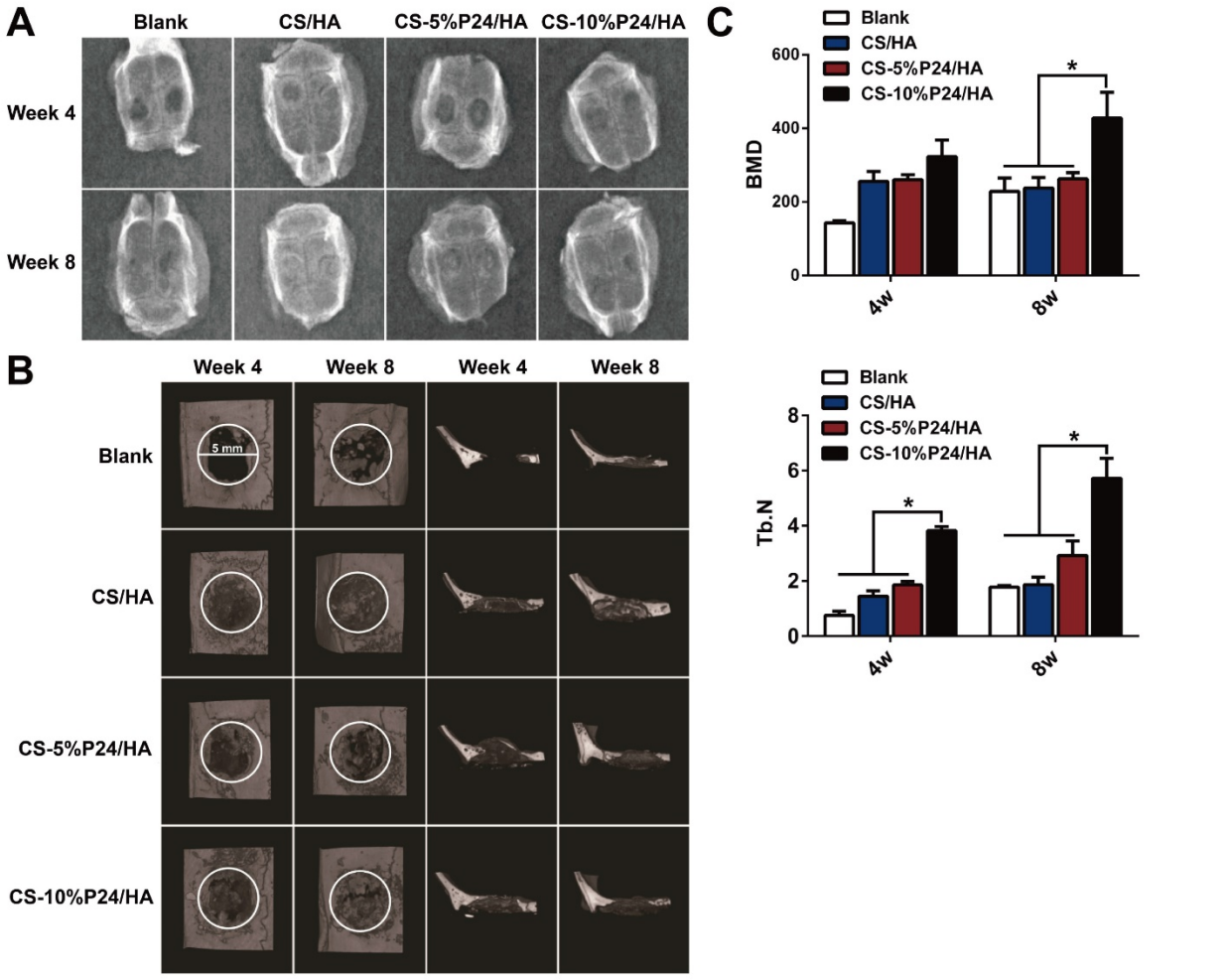

Figure 6. (A) X-ray examination of the whole calvarias post-implantation at weeks 4 and 8 *in vivo*. X-ray examination of the whole calvarias of Blank, CS/HA, CS-5%P24/HA, and CS-10%P24/HA groups, indicating new bone formation at the defects. (B) 3D micro-CT reconstructed images at 4 and 8 weeks with different implants. (C). Micro-CT examination of the whole calvarias after 4 and 8 weeks implantation *in vivo*. Bone mineral density (BMD) and trabecular number (Tb.N). *$p < 0.05$.

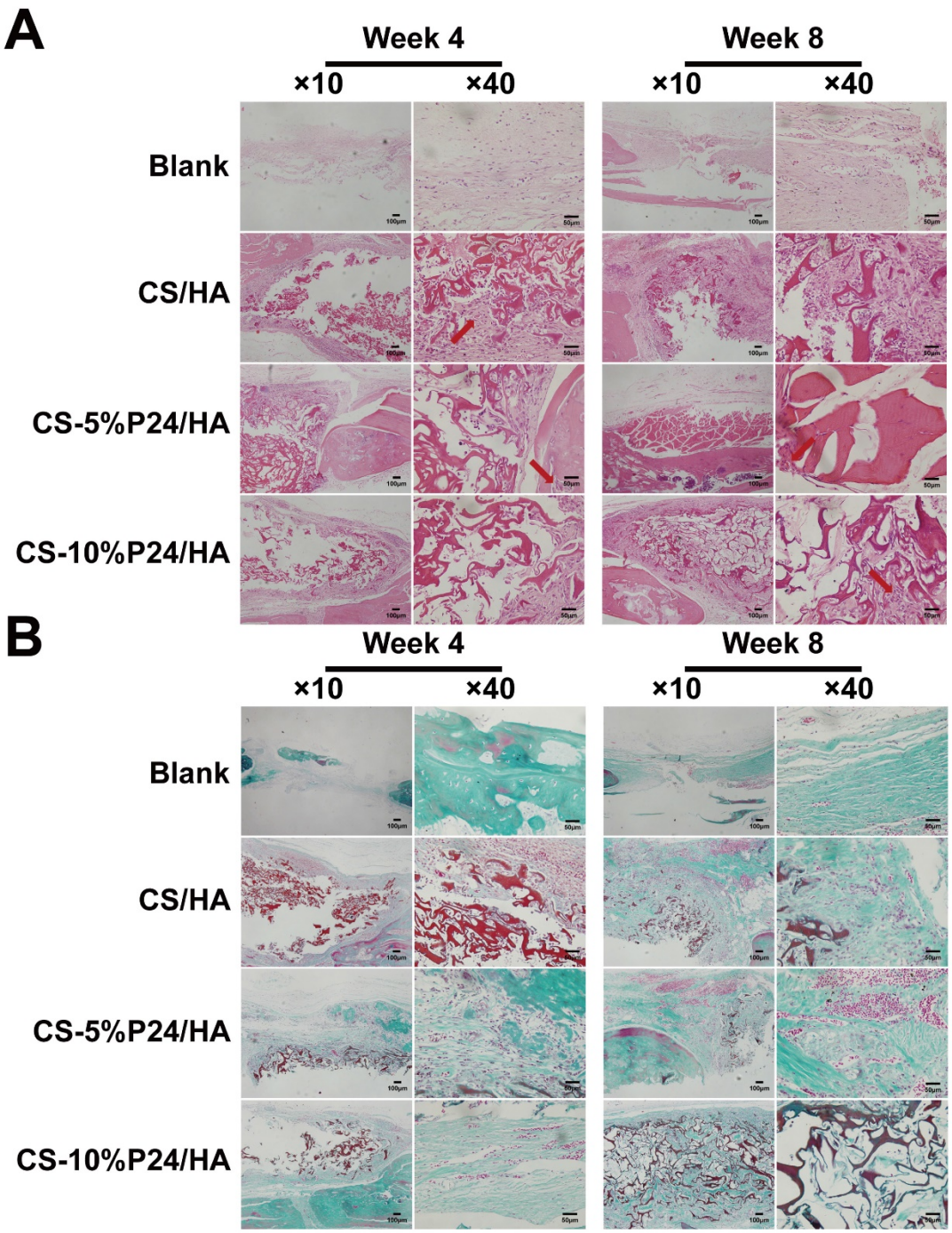

Figure 7. Histology of the repaired calvarias after 4 and 8 weeks implantation *in vivo*. (A) Hematoxylin and eosin staining of the repaired calvarias in Blank, CS/HA, CS-5%P24/HA, and CS-10%P24/HA groups. Red arrows show new formed blood vessels in or around the scaffolds. (B) Masson's staining of the repaired calvarias in Blank, CS/HA, CS-5%P24/HA, and CS-10%P24/HA groups.

Histology

Histological examination revealed the formation of regenerated bone with a typical structure of mature bone in the central part of the repaired area in the CS-P24/HA groups after 4 weeks post-implantation (Fig. 7A). In contrast, no obvious bone, but fibrous tissue was detected in the CS/HA group. For 8 weeks post-implantation, the remaining scaffold materials were detectable in all groups. In contrast to the lack of typical bone formation in the defect area of the blank and the CS/HA group, robust bone formation was found in the repaired area in the CS-5%P24/HA and CS-10%P24/HA groups. Particularly, larger bones were present in the area implanted with CS-10%P24/HA in contrast to small bones in the CS-5%P24/HA and the CS/HA groups (Figs. 7A, 7B). Immunohistochemical analysis showed that the area grafted with CS-P24/HA exhibited high expression

levels of OCN and CD31 and typical osteocytes were observed 8 weeks post-implantation (Fig. 8). Taken together, our results suggest that CS-P24/HA remarkably augments bone regeneration *in vivo.*

Discussion

The efficacy of BMP-2 depends on its mode of delivery. It has been proved long-term delivery of BMP-2 is more effective at enhancing orthotopic bone formation than short-term delivery over a range of doses [32]. At present, one of the key issues regarding BMP-2 is a suitable delivery system that can ensure its long-term controlled release and the bioactivity of BMP-2. In many cases, BMP-2 deposited in the material releases with an early burst, and diffuses away from the implantation site too quickly [33]. Therefore, much attention has been paid to a more reliable vehicle for the sustained delivery of growth factor to target sites. Systems evaluated as vehicles to localize and delivery BMP-2 include porous hydroxyapatite (HA), absorbable collagen, polylactic-co-glycolic acid, et al [33]. Chitosan is a well-tested delivery vehicle as well. Chitosan, obtained by alkaline deacetylation of chitin, is one of the most abundant polysaccharides in nature. However, chitosan suffers from limited solubility at physiological pH and causes presystemic metabolism of drugs in the presence of proteolytic enzymes [34]. These inherent drawbacks of chitosan have been overcome by forming derivatives such as carboxylated, acylated or thiolated chitosan [35]. Among these various chitosan derivates, thiomer technology has a range of advantages for drug delivery such as sustained drug release and high stability [36]. The usefulness of thiolated chitosan as a scaffold for controlled drug release has been demonstrated by means of model drugs such as clotrimazole [37], salmon calcitonin [38] and insulin [39]. However, most of the research has focused on systemic drug delivery. Meanwhile, despite the advantages of thiolated chitosan for tissue engineering, the potential application of this material for bone tissue were rarely investigated.

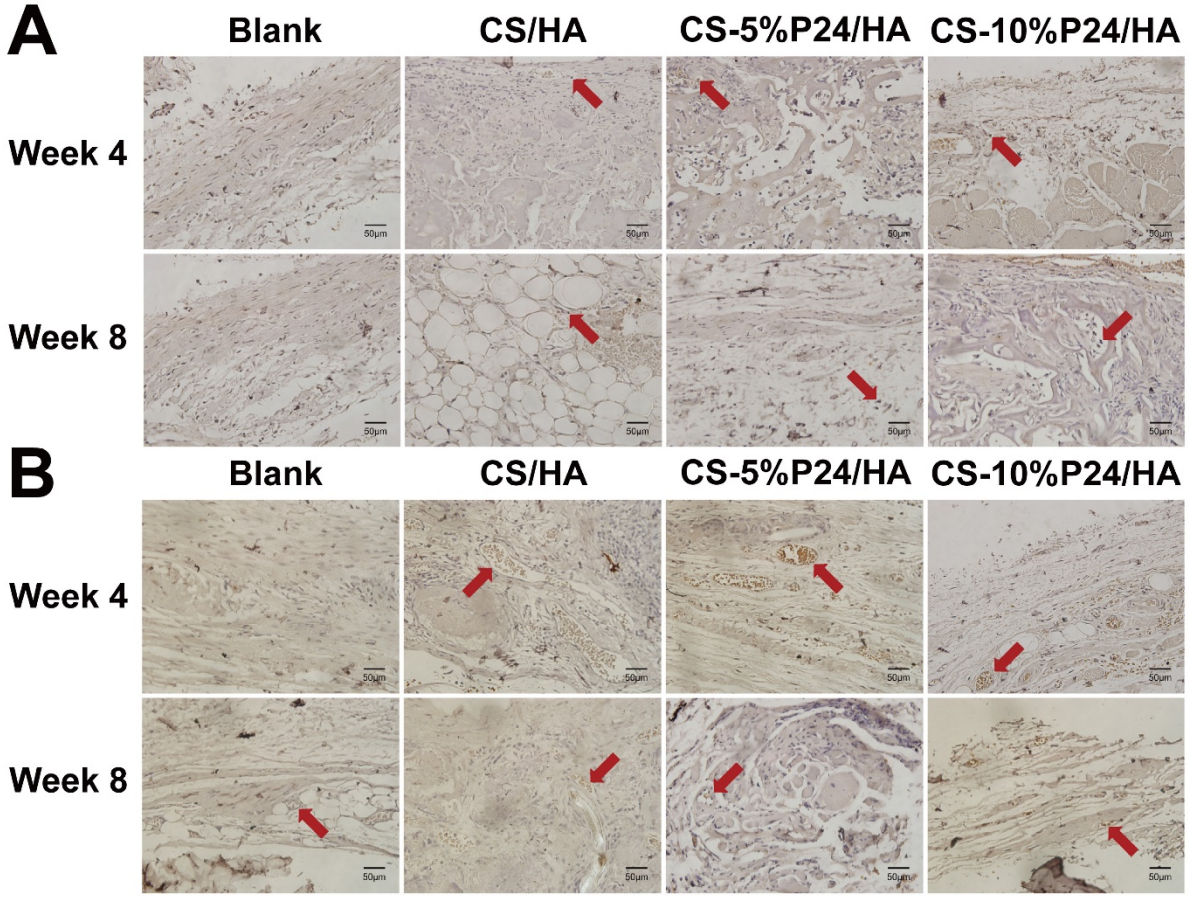

Figure 8. Immunohistology. Cells or areas that appear dark brown represent OCN-positive cells or CD31-positive area, respectively, in (A) and (B), positive area of CD31 indicating the blood vessels in (B), and the areas in white are voids. Representative magnified images are at 40× magnification. Scale bar = 50 μm.

In this study, we developed a new biomimetic composite scaffold for the controlled delivery of BMP2-derived peptide P24 through the chemical modification of chitosan -thiolated chitosan. The cumulative release amounts of P24 from CS-P24/HA revealed no initial burst-release which was quite common for protein release from scaffold functionalized by physical absorption or coating technique [40]. The cumulative release results also indicated that chemical modification technique of thiolated chitosan could more efficiently mediate the grafting of peptides onto scaffolds for BMP-2 peptides delivery compared with physical adsorption. Moreover, using the specific amino acids of P24 for binding to thiolated chitosan might allow for the configuration of immobilized peptides on the scaffold, theoretically, which was impossible to achieve by regular physical adsorption in practice [41, 42]. XPS results characterized the chemical compositions and states of scaffolds with varying amounts of P24 (Fig. 1C). The peak at 166.8 eV (168.0 eV) implied the di-sulfide bonds. The S/C ratio for CS-5%P24/HA and CS-10%P24/HA was 0.64% and 0.92%, respectively. The high amount of amide in CS-P24 was mainly assigned to the existence of the peptide. The increase of the peak intensity for the amide and S/C ratio from CS-5%P24/HA to CS-10%P24/HA both demonstrated the increasing amount of P24 in the scaffolds. The period of sustained release of the BMP-2 peptide continued until day 90 for CS-P24/HA (Fig. 1E), suggesting a strong interaction between the scaffold and the growth factor. Furthermore, the release profiles of CS-5%P24/HA and CS-10%P24/HA were linear and could be fitted according to zero-order kinetic model (R^2=0.9929; R^2=0.9757). Obviously, controlled release of P24 from the porous scaffold through chemical modification of chitosan had been achieved, which mainly relied on the disulfide bonds between thiol groups of thiolated chitosan and P24 (Fig. 1C). In addition, adequate amounts of P24 in CS-P24/HA also contributed to the sustained release. *In vitro*, abundant and even-distributed P24 in CS-P24/HA could be released in stable environment (at 37 °C under continuously shaking for 90 days), without the influence of degradation and remodeling due to complicated environment *in vivo*. Taken together, chemical modification, adequate P24, and stable environment *in vitro* collectively led to the cumulative *in vitro* release of BMP2-derived peptide P24 over a period of 90 days. From the perspective of drug delivery performance, this CS-P24/HA scaffold is adaptable in therapeutic application, because this BMP-2 peptides delivery system can prevent the growth factor from degrading prematurely and enable the local dose to be lowered while guaranteeing long-term delivery and such a retarded therapeutic application is propitious to minimize the risk of undesirable effects such as excessive bone formation and immune response.

Besides the favorable controlled delivery performance, the biological effects of CS-P24/HA scaffold were desirable as it was provided with the osteoconductivity of chitosan/hydroxyapatite and the osteoinductivity of BMP-2 peptides. BMP-2 plays a vital role in osteogenic differentiation [43]. In the present study, P24 was designed as a newly synthesized peptide with 24 amino acids according to the knuckle epitope of BMP-2. This peptide had a relatively small molecular weight with good stability and a linear structure that may easily reduce its biological effect. Meanwhile, the active sites of the short chain polypeptide can be fully exposed. P24 also contained abundant Asp (aspartic acid) and phosphorylated Ser (serine), which promoted and guided mineralization of the natural bone matrix. In addition, similar to BMP-2, P24 might induce transcription factors, such as Runx2, the principal osteogenic master gene for bone formation, constituting a network of activities and molecular switches for bone development and osteoblast differentiation [44]. Runx2 target genes included regulators of cell growth control, components of the bone extracellular matrix, angiogenesis, and signaling proteins for the development of the osteoblast phenotype and bone turnover [44].

The synergistically biological effects of CS-P24/HA scaffold on BMSCs were evaluated from multiple aspects. In this study, the CS-P24/HA scaffold was found to support cell adhesion, spreading, proliferation, and osteogenesis of the rat BMSCs *in vitro*. This scaffold provided an optimal micro-environment for cell attachment and growth. Cells demonstrated larger osteogenic differentiation when they were induced at a higher density. As shown in Fig. 2A, CS-5%P24/HA and CS-10%P24/HA induced higher proliferation of BMSCs than CS/HA. Therefore, these results suggested that the higher proliferation of BMSCs on CS-P24/HA might be attributed to the osteoblastic lineage progression of BMSCs. ALP activity analysis revealed that the BMSCs exhibited higher expression of ALP on CS-P24/HA than that on CS/HA (Fig. 2C). Results from our study showed higher levels of expression of OCN, RUNX-2, and Col-I of BMSCs on CS-P24/HA scaffolds than on CS/HA scaffolds. Wang YK et al. illustrated that cell adhesion to the extracellular matrix (ECM) affects cell shape, cytoskeletal mechanics, BMP-induced signaling, and osteogenic differentiation of hMSCs [45]. They

demonstrated that BMP-2-induced osteogenesis was progressively antagonized with decreased cell spreading and RhoA/ROCK-mediated cytoskeletal tension was directly involved [45]. Moreover, it has been proven that ECM elasticity influences the expression of surface integrin of BMSCs, which in turn can modulate BMP receptor internalization, thereby regulating lineage specification of BMSCs [46].

In vivo osteoinductive studies revealed that the degree of ectopic osteogenesis in the dorsal muscle pocket of rats was significantly higher in the CS-10%P24/HA scaffold than in the CS/HA scaffold. To further evaluate the ability of CS-P24/HA scaffolds to facilitate bone growth *in vivo*, we surgically created cranial bone defects in SD rats. The *in-vivo* study showed that new bone-like tissue determined by micro-CT, combined with histological examination and immunohistochemical analysis, was significantly increased in the CS-P24/HA groups than in the CS/HA group *in vivo* (Figs. 6-8). The intensity of the defect was also higher in the CS-P24/HA groups compared to the CS/HA group (Fig. 6). The *in vivo* full-thickness cranial bone defect model repair further demonstrated that CS-P24/HA was superior to CS/HA in promoting bone regeneration, which was likely due to the role of CS-P24/HA in facilitating osteogenic differentiation in BMSCs as well as supporting BMSC adhesion, spreading, and proliferation, just as described *in vitro*. Therefore, in our study, the BMSCs might contribute to bone repair in two different ways: first, BMSCs might directly differentiate into the osteocytes; second, they might modify the healing environment by secreting a number of trophic molecules, such as soluble extracellular matrix glycoproteins, cytokines, and growth factors [47]. The contribution of the BMSCs to bone repair and regeneration could be elucidated from the expression of markers and ECM synthesis (Fig. 2, Fig. 4 and Fig. 8). In this study, osteogenic ECM gene markers, OCN were up-regulated in both CS-5%P24/HA and CS-10%P24/HA groups. However, further investigation is necessary to fully illustrate the role of BMSCs influenced by CS-P24/HA in bone regeneration *in vivo*.

Conclusions

A chitosan-P24/hydroxyapatite (CS-P24/HA) controlled delivery scaffold was created by the chemical modification technique and was found to steadily release P24 for 90 days, furthermore, the release profiles of CS-5%P24/HA and CS-10%P24/HA were linear and could be fitted according to zero-order kinetic model (R2=0.9929; R2=0.9757);. It was demonstrated to support BMSC adhesion and spreading and promote cell viability and proliferation. Furthermore, CS-P24/HA induced osteogenic differentiation of BMSCs both *in vitro* and *in vivo*. Finally, CS-P24/HA was superior to CS/HA in promotion of bone regeneration *in vivo*. This study highlights the enormous potential of using the CS-P24/HA scaffold for bone tissue engineering applications.

Acknowledgments

The authors are grateful for the financial support from the National Natural Science Foundation of China (no.81371931 and no.81301240), the Natural Science Foundation of Guangdong Province, China (no.2014A030313352 and no.2014A030313310) and the Shenzhen Strategic Emerging Industries Project (CXZZ20130517095548798).

Competing Interests

The authors have declared that no competing interest exists.

References

1. Lee K, Silva EA, Mooney DJ. Growth factor delivery-based tissue engineering: general approaches and a review of recent developments. J R Soc Interface. 2011; 8: 153-70.
2. Cao H, Chen MM, Liu Y, Liu YY, Huang YQ, Wang JH, et al. Fish collagen-based scaffold containing PLGA microspheres for controlled growth factor delivery in skin tissue engineering. Colloids Surf B Biointerfaces. 2015; 136: 1098-106.
3. Sarti F, Bernkop-Schnürch A. Chitosan and Thiolated Chitosan. Advances in Polymer Science. 2011; 243: 93-110.
4. Kafedjiiski K, Krauland AH, Hoffer MH, Bernkop-Schnürch A. Synthesis and in vitro evaluation of a novel thiolated chitosan. Biomaterials. 2005; 26: 819-26.
5. Matsuda A, Kobayashi H, Itoh S, Kataoka K, Tanaka J. Immobilization of laminin peptide in molecularly aligned chitosan by covalent bonding. Biomaterials. 2005; 26: 2273-9.
6. Liu X, Chen Y, Huang Q, He W, Feng Q, Yu B. A novel thermo-sensitive hydrogel based on thiolated chitosan/hydroxyapatite/beta-glycerophosphate. Carbohydr Polym. 2014; 110: 62-9.
7. Li L, Zhou G, Wang Y, Yang G, Ding S, Zhou S. Controlled dual delivery of BMP-2 and dexamethasone by nanoparticle-embedded electrospun nanofibers for the efficient repair of critical-sized rat calvarial defect. Biomaterials. 2015; 37: 218-29.
8. Kaneko H, Arakawa T, Mano H, Kaneda T, Ogasawara A, Nakagawa M, et al. Direct stimulation of osteoclastic bone resorption by bone morphogenetic protein (BMP)-2 and expression of BMP receptors in mature osteoclasts. Bone. 2000; 27: 479-86.
9. Raida M, Heymann AC, Gunther C, Niederwieser D. Role of bone morphogenetic protein 2 in the crosstalk between endothelial progenitor cells and mesenchymal stem cells. Int J Mol Med. 2006; 18: 735-9.
10. Murphy CM, Schindeler A, Gleeson JP, Yu NY, Cantrill LC, Mikulec K, et al. A collagen-hydroxyapatite scaffold allows for binding and co-delivery of recombinant bone morphogenetic proteins and bisphosphonates. Acta Biomater. 2014; 10: 2250-8.
11. Suliman S, Xing Z, Wu X, Xue Y, Pedersen TO, Sun Y, et al. Release and bioactivity of bone morphogenetic protein-2 are affected by scaffold binding techniques in vitro and in vivo. J Control Release. 2015; 197: 148-57.
12. Seol YJ, Park YJ, Lee SC, Kim KH, Lee JY, Kim TI, et al. Enhanced osteogenic promotion around dental implants with synthetic binding motif mimicking bone morphogenetic protein (BMP)-2. J Biomed Mater Res A. 2006; 77: 599-607.
13. Suzuki Y, Tanihara M, Suzuki K, Saitou A, Sufan W, Nishimura Y. Alginate hydrogel linked with synthetic oligopeptide derived from BMP-2 allows ectopic osteoinduction in vivo. J Biomed Mater Res. 2000; 50: 405-9.
14. Lin X, Zamora PO, Albright S, Glass JD, Pena LA. Multidomain synthetic peptide B2A2 synergistically enhances BMP-2 in vitro. J Bone Miner Res. 2005; 20: 693-703.
15. Li J, Hong J, Zheng Q, Guo X, Lan S, Cui F, et al. Repair of rat cranial bone defects with nHAC/PLLA and BMP-2-related peptide or rhBMP-2. J Orthop Res. 2011; 29: 1745-52.

16. Wu B, Zheng Q, Guo X, Wu Y, Wang Y, Cui F. Preparation and ectopic osteogenesis in vivo of scaffold based on mineralized recombinant human-like collagen loaded with synthetic BMP-2-derived peptide. Biomed Mater. 2008; 3: 044111.
17. Tam JP, Wu CR, Liu W, ZhanG JW. Disulfide Bond Formation In Peptides By Dimethyl-Sulfoxide - Scope And Applications. J Am Chem Soc. 1991; 113: 6657-62.
18. Yu B, Zhang Y, Li X, Wang Q, Ouyang Y, Xia Y, et al. The Use of Injectable Chitosan/Nanohydroxyapatite/Collagen Composites with Bone Marrow Mesenchymal Stem Cells to Promote Ectopic Bone Formation In Vivo. J Nanomater. 2013, 2013(3):3805-3816.
19. Sawyer AA, Song SJ, Susanto E, Chuan P, Lam CXF, Woodruff MA, et al. The stimulation of healing within a rat calvarial defect by mPCL-TCP/collagen scaffolds loaded with rhBMP-2. Biomaterials. 2009; 30: 2479-88.
20. Ma Y, Zhang W, Wang Z, Wang Z, Xie Q, Niu H, et al. PEGylated poly(glycerol sebacate)-modified calcium phosphate scaffolds with desirable mechanical behavior and enhanced osteogenic capacity. Acta Biomater. 2016; 44: 110-24.
21. Taniyama K, Shirakata Y, Yoshimoto T, Takeuchi N, Yoshihara Y, Noguchi K. Bone formation using beta-tricalcium phosphate/carboxymethyl-chitin composite scaffold in rat calvarial defects. Oral Surg Oral Med Oral Pathol Oral Radiol. 2013; 116: e450-6.
22. Masuko T, Iwasaki N, Yamane S, Funakoshi T, Majima T, Minami A, et al. Chitosan-RGDSGGC conjugate as a scaffold material for musculoskeletal tissue engineering. Biomaterials. 2005; 26: 5339-47.
23. Bernkop-Schnurch A, Hornof M, Zoidl T. Thiolated polymers--thiomers: synthesis and in vitro evaluation of chitosan-2-iminothiolane conjugates. Int J Pharm. 2003; 260: 229-37.
24. He G, Chen X, Yin Y, Zheng H, Xiong X, Du Y. Synthesis, characterization and antibacterial activity of salicyloyl chitosan. Carbohydr Polym. 2011; 83: 1274-8.
25. Lawrie G, Keen I, Drew B, Chandler-Temple A, Rintoul L, Fredericks P, et al. Interactions between alginate and chitosan biopolymers characterized using FTIR and XPS. Biomacromolecules. 2007; 8: 2533-41.
26. Huang QZ, Wang SM, Huang JF, Zhuo LH, Guo YC. Study on the heterogeneous degradation of chitosan with hydrogen peroxide under the catalysis of phosphotungstic acid. Carbohydr Polym. 2007; 68: 761-5.
27. Fan L, Wu H, Cao M, Zhou X, Peng M, Xie W, et al. Enzymatic synthesis of collagen peptide-carboxymethylated chitosan copolymer and its characterization. React Funct Polym. 2014; 76: 26-31.
28. Fan L, Wu H, Zhou X, Peng M, Tong J, Xie W, et al. Transglutaminase-catalyzed grafting collagen on chitosan and its characterization. Carbohydr Polym. 2014; 105: 253-9.
29. Unsoy G, Yalcin S, Khodadust R, Gunduz G, Gunduz U. Synthesis optimization and characterization of chitosan-coated iron oxide nanoparticles produced for biomedical applications. J Nanopart Res. 2012, 14(11):1-13.
30. Wang Y, Li B, Zhou Y, Jia D, Song Y. CS-Fe(II,III) complex as precursor for magnetite nanocrystal. Polym Advan Technol. 2011; 22: 1681-4.
31. Iucci G, Dettin M, Battocchio C, Gambaretto R, Di Bello C, Polzonetti G. Novel immobilizations of an adhesion peptide on the TiO2 surface: An XPS investigation. Mat Sci Eng C-Mater. 2007; 27: 1201-6.
32. La WG, Kang SW, Yang HS, Bhang SH, Sun HL, Park JH, et al. The Efficacy of Bone Morphogenetic Protein-2 Depends on Its Mode of Delivery. Artif Organs. 2010; 34: 1150-3.
33. Rambhia KJ, Ma PX. Controlled drug release for tissue engineering. J Control Release. 2015; 219: 119-28.
34. Logithkumar R, Keshavnarayan A, Dhivya S, Chawla A, Saravanan S, Selvamurugan N. A review of chitosan and its derivatives in bone tissue engineering. Carbohydr Polym. 2016; 151: 172-88.
35. Chen MC, Mi FL, Liao ZX, Hsiao CW, Sonaje K, Chung MF, et al. Recent advances in chitosan-based nanoparticles for oral delivery of macromolecules. Adv Drug Deliver Rev. 2013; 65: 865-79.
36. Bhattarai N, Gunn J, Zhang M. Chitosan-based hydrogels for controlled, localized drug delivery. Adv Drug Deliver Rev. 2010; 62: 83-99.
37. Kast CE, Valenta C, Leopold M, Bernkop-Schnürch A. Design and in vitro evaluation of a novel bioadhesive vaginal drug delivery system for clotrimazole. J Control Release. 2002; 81: 347-54.
38. Guggi D, Krauland AH, Bernkop-Schnürch A. Systemic peptide delivery via the stomach: in vivo evaluation of an oral dosage form for salmon calcitonin. J Control Release. 2003; 92: 125-35.
39. Yin L, Ding J, He C, Cui L, Tang C, Yin C. Drug permeability and mucoadhesion properties of thiolated trimethyl chitosan nanoparticles in oral insulin delivery. Biomaterials. 2009; 30: 5691-700.
40. Park YJ, Kim KH, Lee JY, Ku Y, Lee SJ, Min BM, et al. Immobilization of bone morphogenetic protein-2 on a nanofibrous chitosan membrane for enhanced guided bone regeneration. Biotechnol Appl Bioc. 2006; 43: 17–24.
41. Lee H, Rho J, Messersmith PB. Facile Conjugation of Biomolecules onto Surfaces via Mussel Adhesive Protein Inspired Coatings. Adv Mater. 2009; 21: 431–4.
42. King WJ, Krebsbach PH. Growth factor delivery: How surface interactions modulate release in vitro and in vivo. Adv Drug Deliver Rev. 2012; 64: 1239-56.
43. Liu H, Peng H, Wu Y, Zhang C, Cai Y, Xu G, et al. The promotion of bone regeneration by nanofibrous hydroxyapatite/chitosan scaffolds by effects on integrin-BMP/Smad signaling pathway in BMSCs. Biomaterials. 2013; 34: 4404-17.
44. Lian JB, Stein GS, Javed A, van Wijnen AJ, Stein JL, Montecino M, et al. Networks and hubs for the transcriptional control of osteoblastogenesis. Rev Endocr Metab Disord. 2006; 7: 1-16.
45. Wang YK, Yu X, Cohen DM, Wozniak MA, Yang MT, Gao L, et al. Bone morphogenetic protein-2-induced signaling and osteogenesis is regulated by cell shape, RhoA/ROCK, and cytoskeletal tension. Stem Cells Dev. 2012; 21: 1176-86.
46. J D, Chen X, Liang X, Zhang G, Xu J, He L, et al. Integrin activation and internalization on soft ECM as a mechanism of induction of stem cell differentiation by ECM elasticity. Proc Natl Acad Sci U S A. 2011; 108: 9466-71.
47. Ankrum J, Karp JM. Mesenchymal stem cell therapy: Two steps forward, one step back. Trends Mol Med. 2010; 16: 203-9.